

# Diffraction of correlated biphotons through transparent samples

Nazanin Dehghan,<sup>1,2</sup> Alessio D’Errico,<sup>1,2,\*</sup> Yingwen Zhang,<sup>1,2</sup> and Ebrahim Karimi<sup>1,2,3</sup>

<sup>1</sup>*Nexus for Quantum Technologies, University of Ottawa, Ottawa, K1N 6N5, ON, Canada*

<sup>2</sup>*National Research Council of Canada, 100 Sussex Drive, K1A 0R6, Ottawa, ON, Canada*

<sup>3</sup>*Institute for Quantum Studies, Chapman University, Orange, California 92866, USA*

Two-photon states generated through degenerate spontaneous parametric down-conversion (SPDC) can exhibit sharp correlations in the transverse spatial coordinates. This effect, associated with the separability of the biphoton wavefunction into functions of the centroid and the difference coordinates, leads to unique free space propagation features. Here, we show that if a phase object is placed in the image plane of the source, only the propagation of the function of the centroid coordinates is altered. This propagation can be experimentally reconstructed in coincidence imaging and via post-selection on spatially correlated events, which will reveal the diffraction pattern from the object with a phase enhancement due to the probe’s two-photon nature. Our findings offer applications for non-interferometric, quantum-enhanced phase imaging.

## I. INTRODUCTION

Among the most intriguing applications of structured quantum light [1–4] is the possibility of exploiting correlations between optical modes in two or more photon states to boost the sensitivity of measurements beyond the limits allowed by classical states of light [5]. Quantum metrology based on nonclassical light has found applications exploiting squeezed states [6, 7], N00N states [8–10], as well as induced coherence [11] to enhance phase sensitivity in optical interferometers or in imaging apparatuses [12–16], to increase the resolution of imaging systems [17–19] and to resolve coherent [20, 21] or incoherent [22] displacements. The most used probe for quantum imaging is the quantum state generated by spontaneous parametric down-conversion (SPDC). The non-classical features of this state allow accessing a broad range of quantum-enhanced measuring strategies using correlations in polarization [8, 15, 23], photon number [24], spatial modes [25–28], transverse position and/or momentum [1, 29] as well as in frequency [30].

Towards imaging applications, spatial correlations in position and anticorrelations in momentum spaces have been exploited in quantum ghost imaging experiments and can be extended to the two-color regime when also spectral correlations are exploited [30]. While ghost imaging is based on triggering a pixelated detector with a bucket detector, other experiments make use of either post-selection on single spatial modes instead of the bucket detector [31] or the reconstruction of spatially resolved coincidences. The latter approach has sparked a wide range of imaging applications based on coincidence analysis: quantum digital holography [15, 23, 32, 33], spatially and spectrally resolved Hong-Ou-Mandel interferometry [34–36], pixel super-resolution imaging [37, 38], light-field microscopy [39, 40], hyperspectral imaging [41], and high dimensional quantum state characterisation [33, 42, 43]. Most of these works have been allowed by different camera technologies, which effectively allow spatially resolved coincidences without the need for raster scanning; these are based on either EMCCD cameras [44], SPAD arrays [45] and event-

based intensified cameras [46, 47]. In particular, event-based cameras allow for a fast acquisition rate with the ability to resolve spatial correlations in fractions of seconds, thus allowing for data collection in relatively short times when compared with other detectors. Their use allowed for developing new methods of quantum state characterisation based on interferometry [33], spatially resolved polarisation tomography [42] and non-interferometric biphoton state phase retrieval [43]. The latter approach showed that post-selecting the distribution of two-photon coincidences on spatially correlated events, it is possible to isolate the contribution to the biphoton state due to the pump amplitude from the contribution due to the phase matching function. This effect is related to the fact that the pump field coherence properties are transferred in the two-photon spatial correlations, as demonstrated experimentally in Refs. [43, 48]. In this work, we demonstrate that this approach can be used to reveal the diffraction of correlated biphoton states through a transparent sample –placed after the down-conversion crystal– with varying thickness and/or refractive index. The proposed technique is based on placing the sample in the near field of the nonlinear crystal, generating the two-photon state, and collecting spatially resolved coincidence events in different planes away from the sample. Typically, only looking at the distribution of two-photon coincidences would not provide the structure of the sample. However, we show that by post-selecting the coincidences dataset on spatially correlated events, a pattern appears that can be associated with the intensity distribution of a coherent light beam –with the wavelength of the pump laser– diffracted from the sample, but as if the sample imparted phase was doubled, a phase enhancement effect due to the two-photon spatial correlations. These results, integrated with quantitative phase retrieval techniques, could lead to novel applications in quantum-enhanced phase imaging.

## II. THEORY

Two-photon states with high spatial correlation can be generated by pumping a thin non-linear crystal (thickness  $\approx 1$  mm) with a collimated pump laser. In the degenerate case, where the two photons are emitted at the same frequency, the two-photon

\* [aderrico@uottawa.ca](mailto:aderrico@uottawa.ca)

wavefunction in the transverse momentum space reads [1, 33]:

$$\psi(\mathbf{k}_s, \mathbf{k}_i) = \text{sinc}\left(\frac{L\lambda_p}{4\pi}|\mathbf{k}_s - \mathbf{k}_i|^2 + \xi\right)\mathcal{A}(\mathbf{k}_s + \mathbf{k}_i), \quad (1)$$

where  $L$  is the crystal thickness,  $\lambda_p$  the central wavelength of the pump laser,  $\mathbf{k}_{s,i} = (k_{x_{s,i}}, k_{y_{s,i}})$  refers to the transverse wavevector components of signal ( $s$ ) and idler ( $i$ ) photons,  $\xi$  is the longitudinal walk-off which can be tuned changing the orientation of the optical axis of the crystal, and  $\mathcal{A}$  is proportional to the angular spectrum amplitude of the pump laser field. The sinc function corresponds to the phase-matching contribution to the biphoton wavefunction. Equation (1) is equivalent to the far field structure of the bi-photon wavefunction. The spatial structure of the near field can thus be derived by the Fourier transform of  $\psi(\mathbf{k}_s, \mathbf{k}_i)$ . The phase matching in the near-field will give a narrow contribution of width  $\sim \sqrt{L\lambda_p/4\pi}$ , which is typically of the order of a few  $\mu\text{m}$ . The pump laser width in the near field can be assumed to be on the order of the crystal transverse size (a few mm). Hence, we can approximate the biphoton state in the nearfield as

$$|\psi\rangle = \int \tilde{\mathcal{A}}(\mathbf{x})\hat{a}_{\mathbf{x}}^{\dagger 2} d^2x |0\rangle, \quad (2)$$

where  $\hat{a}_{\mathbf{x}}^{\dagger}$  is a photon creation operator in the transverse position  $\mathbf{x}$ ,  $\tilde{\mathcal{A}}$  is the Fourier transform of  $\mathcal{A}$ , and  $|0\rangle$  is the vacuum state. Consider a sample placed in this plane with spatially variable transmittance and thickness (or variable refractive index). The sample's action can be modeled as the following transformation on the creation operators:

$$\hat{a}_{\mathbf{x}}^{\dagger} \rightarrow t(\mathbf{x})\hat{a}_{\mathbf{x}}^{\dagger} + i\sqrt{1 - T(\mathbf{x})}\hat{a}_{\text{loss}}^{\dagger}, \quad (3)$$

where  $t(\mathbf{x}) := \sqrt{T(\mathbf{x})}e^{i\alpha(\mathbf{x})}$  is a function whose modulus square is the power transmittance  $T(\mathbf{x})$  of the object and whose phase  $\alpha(\mathbf{x})$  is related to the spatially varying thickness and/or refractive index. The term  $\sqrt{1 - T(\mathbf{x})}\hat{a}_{\text{loss}}^{\dagger}$  takes into account the reflected or absorbed photons, as scattered to undetected modes represented by the operator  $\hat{a}_{\text{loss}}^{\dagger}$ . The part of the wavefunction that contributes to coincidence measurements is,

$$|\psi\rangle = \int \tilde{\mathcal{A}}(\mathbf{x})t^2(\mathbf{x})\hat{a}_{\mathbf{x}}^{\dagger 2} d^2x |0\rangle. \quad (4)$$

The above equation shows how the effect of the sample on the biphoton state is to modify the pump amplitude function  $\tilde{\mathcal{A}}$  as  $\tilde{\mathcal{A}} \rightarrow t^2\tilde{\mathcal{A}} = T\tilde{\mathcal{A}}e^{i2\alpha}$ , which appears as if the field passed through a sample with squared power transmittance and doubled phase. A coincidence image collected in the image plane would show only the effect of the power transmittance  $T$  but not of the phase. To observe the effects of the phase, one could perform an interferometric measurement based on the technique presented in Ref. [33] or observe the free-space propagation of the biphoton state as in Ref. [43]. Here, we will follow the second approach. As shown in Ref. [43], the propagation of the biphoton wavefunction can be modelled as two independent Fresnel propagators applied to the phase matching and the pump wavefunctions. More precisely, let

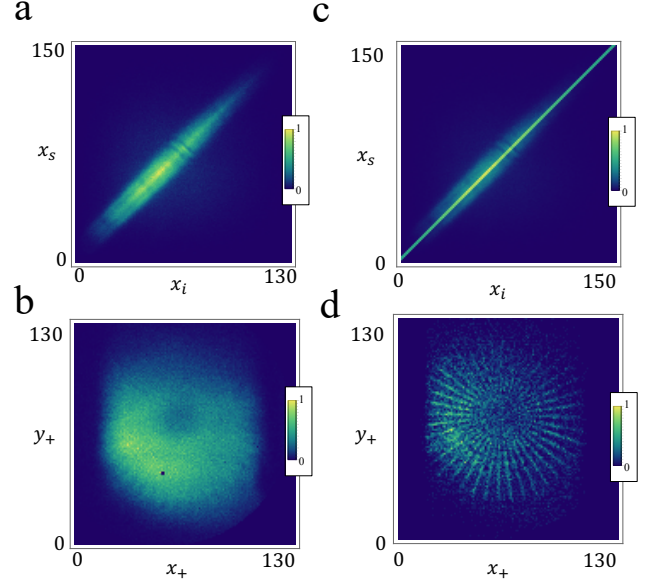


Figure 1. **Extraction of centroid coincidence image.** Panel a shows experimentally observed  $x$ -correlations in a plane that is 1 cm away from the sample ( $y$ -correlations have a similar width). If events are selected under the only restriction of being separated by less than 10 ns time delay, the spatial distribution of events is shown in panel b. However, if we also select events where signal and idler photons hit the sensor in the same transverse position, up to a fixed shift, – as highlighted by the yellow line in panel b –, then the distribution of events will yield the “centroid coincidence image” shown in d. The sample features appear as a consequence of the diffraction phenomena described by Eq. (7). Coordinate ticks are in pixels (pixel size = 55  $\mu\text{m}$ )

$\mathbf{X}_{i,s}$  be the transverse coordinates in a plane at a distance  $z$  from the crystal and  $\mathbf{X}'_{i,s}$  the transverse coordinates in a plane at a distance  $z'$ . In  $z$ , the biphoton wavefunction has a form similar to Eq. (2):  $\psi_z(\mathbf{X}_i, \mathbf{X}_s) = \Phi(\mathbf{X}_-)\mathcal{E}(\mathbf{X}_+)$ , with  $\mathbf{X}_{\pm} := \mathbf{X}_i \pm \mathbf{X}_s$ . The biphoton wavefunction in  $z'$  is related to the wavefunction in  $z$  by the relation:

$$\psi'_{z'}(\mathbf{X}'_i, \mathbf{X}'_s) = \mathbf{F}[\Phi](\mathbf{X}'_-)\mathbf{F}[\mathcal{E}](\mathbf{X}'_+), \quad (5)$$

where  $\mathbf{F}$  is the Fresnel propagator

$$\mathbf{F}[g](\mathbf{r}') := \int e^{i\frac{\pi}{\lambda_p} \frac{|\mathbf{r}' - \mathbf{r}|^2}{(z' - z)}} g(\mathbf{r}) d^2r. \quad (6)$$

In the present case  $\mathcal{E} = t^2\tilde{\mathcal{A}}$ , thus, the sample placed in the near field will influence the propagation of the centroid contribution of the biphoton, given, in general, by

$$\mathbf{F}[\mathcal{E}](\mathbf{x}') := \int e^{i\frac{\pi}{\lambda_p z'} |\mathbf{x}' - \mathbf{x}|^2} t^2(\mathbf{x})\tilde{\mathcal{A}}(\mathbf{x}) d^2x. \quad (7)$$

The absolute value of this contribution can be experimentally isolated from  $\mathbf{F}[\Phi]$  performing spatially resolved coincidence measurements and postselecting on spatially correlated events, i.e. those events where the idler photon is detected

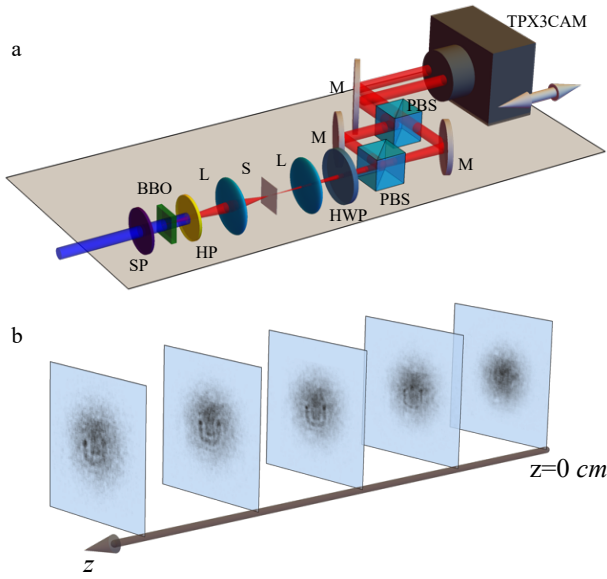


**Figure 2. Experimental setup and extracted biphoton diffraction patterns.** **a.** Sketch of the experimental setup. A collimated pump laser is incident on a Type-I BBO crystal and generates photon pairs. After removing the pump with a high-pass spectral filter (HP), the SPDC probe is sent to a sample (S) in the image plane of the crystal. With 50% probability, the idler and signal photons are sent on two different regions of a time stamping camera (TPX3CAM), using a half-wave plate (HWP) and a polarizing beamsplitter (PBS). The camera is translated along the propagation direction allowing for the acquisition of coincidence images at different propagation planes. M, Mirror. L,  $4 - f$  imager -represented as a lens object. **b.** Centroid coincidence images were obtained at different propagation planes for a sample displaying a  $\pi/4$  phase jump in an “U” shaped region. At  $z = 0$  no structure is discernible. However, in subsequent planes, the diffraction from the phase structure appears.

in  $\mathbf{x}_i$  and the signal photon in  $\mathbf{x}_s = \mathbf{x}_i + \mathbf{c}$ , where  $\mathbf{c}$  is a constant shift that can be chosen at will. This procedure is detailed in Ref. [43] and briefly illustrated in Fig. 1: coincidence events are recorded as a function of signal and idler coordinates  $\mathcal{C}(\mathbf{X}_+, \mathbf{X}_-) = |\mathbf{F}[\Phi](\mathbf{X}_-)|^2 |\mathbf{F}[\mathcal{E}](\mathbf{X}_+)|^2$ . If no further postselection is applied on the events, and the spatial correlations are not sharp due to the free space propagation (as in Fig. 1-a), the spatial distribution of events, called “coincidence image”, will generally appear as in Fig. 1-b. From  $\mathcal{C}$ , we can extract the section  $\int \mathcal{C}(\mathbf{X}_+, \mathbf{X}_-) \delta(\mathbf{X}_-) d^2 X_- \propto |\mathbf{F}[\mathcal{E}](\mathbf{X}_+)|^2$ . In the following, we will refer to the extracted function as the “centroid coincidence image”. An example is illustrated in Fig. 1-d, which clearly shows the appearance of a pattern due to the phase sample. Performing this analysis in different propagation planes, one can thus observe a correlation image that is proportional to the diffraction pattern of the sample. As a consequence, the shape of a phase-only object can be revealed by postselected coincidence image analysis performed in a plane away from the object.

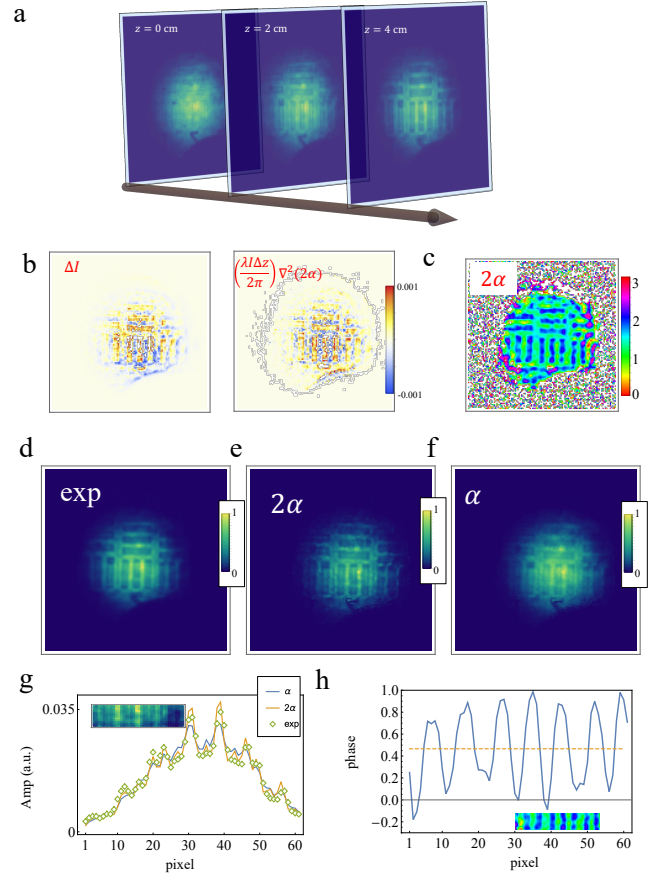


**Figure 3. Phase retrieval from de-focused Centroid Coincidence Images and benchmarking of phase-enhancement.** Panel **a** shows centroid coincidence images captured at different propagation distances from the image plane of a phase target with a depth of 127 nm or a phase of 0.46. Panel **b** illustrates the experimental difference of intensities  $\Delta I$  between the first two planes compared with the expected  $\Delta I$  using the retrieved phase, shown in panel **c**. Panel **d** shows the experimentally captured intensity image at the third plane ( $z = 4$  cm) compared with the intensity obtained from numerically propagated fields with the phase distribution in **c** rescaled. The best result is obtained when the phase variation is close to  $\Delta\phi = 2\alpha = 0.92$  (panel **e**), while the intensity distribution that would have been obtained for a single photon or a coherent laser beam is shown in panel **f**. As highlighted in **g** (the intensities are compared along the region shown in the inset, after summing along the vertical direction), the experimentally captured centroid coincidence image is in better agreement with that expected from an  $\alpha = 0.92$  phase variation. Panel **h** shows the phase variation across the recovered phase image in **c** (the plot is an average of the inset figure). The dashed line is a guide for the eye corresponding to the phase variation of 0.46. The pixel size is  $55 \mu\text{m}$ .

### III. EXPERIMENT

We verify our prediction on the biphoton diffraction by a transparent object exploiting a time stamping camera (TPX3CAM). The TPX3CAM provides nanosecond temporal resolution on each  $256 \times 256$  pixels thus allowing the time

and spatial correlation between SPDC photons to be measured simultaneously. The setup is sketched in Fig. 2-a. A pump laser (405 nm wavelength) is incident on a 1-mm-thick Type-I BBO crystal and generates frequency-degenerate (810 nm) photon pairs via SPDC. The photons are then used to illuminate a sample placed in the image plane of the crystal through a 4-f lens system. Figure 2-b shows an example of the centroid coincidence image, reconstructed by translating the camera along the propagation direction  $z$ , with steps of 5 cm. The sample is a nematic liquid crystal layer electrically tuned to  $\pi$  retardation and with a patterned optical axis obtained using a photoalignment technique [49]. The pattern considered is a “U” shape with a  $\pi/8$  tilt of the optical axis inside the letter and a 0 tilt outside. This translates into a  $\pi/4$  phase jump for an incident left circularly polarized photon, and – from Eq. (4) – a  $\pi/2$  jump for left circularly polarised biphotons. It is evident from Fig. 2-b that while no structure is discernible in the image plane of the sample, the diffraction pattern due to the phase jump becomes visible in subsequent propagation planes.

We conducted a more quantitative analysis on another sample with varying thicknesses. The sample is a phase calibration target introduced in Ref.[50] with depth variations of  $d = 127$  nm and refractive index  $\sim 1.47$ . For a single photon (with wavelength 810 nm) crossing the sample, this amounts to a phase change of  $\alpha \approx 2\pi(1.47 - 1)d/\lambda = 0.46$ , while for correlated biphotons, from Eq. (4), we expect an enhancement in the phase change to  $2\alpha = 0.92$ . Fig. 3-a shows the collected centroid coincidence image at different distances from the sample image plane. For each plane, data were collected for 400 seconds.

We exploit the intensity variation  $\Delta I$  between the first two planes to retrieve the phase pattern using the transport of intensity equation (TIE) [51, 52]

$$\frac{dI}{dz} = \frac{\lambda}{2\pi} I \nabla_{\perp}^2 \phi \quad (8)$$

where  $\phi$  is the unknown phase, and  $\nabla_{\perp}^2$  is the Laplacian in the transverse coordinates. The TIE is valid for paraxial propagation of fields with irrotational phase and uniform intensity and is equivalent to a Poisson equation for the phase with the source given by the longitudinal intensity variation. It can be thus inverted via Fourier transform and using the Green function of the Poisson equation  $K(k_x, k_y) \propto 1/(k_x^2 + k_y^2 + \epsilon)$ , where  $(k_x, k_y)$  are the coordinates in the Fourier space and  $\epsilon$  a regularization factor needed to account for the divergence of  $K$  in the origin. We choose the value  $\epsilon \sim 20$  which minimizes the difference between  $\Delta I$  and  $\Delta z \frac{\lambda}{2\pi} I \nabla_{\perp}^2 \phi$ . The two quantities

are shown in Fig. 3-b. Most of the differences between the two plots are due to noise and the assumption of uniform intensity. Fig. 3-c shows the reconstructed phase pattern. To confirm the phase enhancement we simulate the propagation from  $z = 0$  to  $z = 4$  cm (corresponding to the third plane) and compare it with the corresponding experimental result (Fig. 3-c). The best agreement is found when assuming a phase variation of  $2\alpha \approx 0.92$  (Fig. 3-e) as expected from the biphoton nature of the probe, while a probe experiencing a phase variation  $\alpha \approx 0.46$  would display the diffraction pattern in Fig. 3-f. This is shown more explicitly in Fig. 3-g where the cross-section of the experimentally measured phase target amplitude image at  $z = 4$  cm is compared to the expected cross-section when assuming a phase variation of 0.92 and 0.46. Figure 3-h shows the cross-section of the recovered phase image showing clearly a phase variation of  $\sim 0.9$ .

#### IV. CONCLUSIONS

We have demonstrated that when SPDC states with sharp spatial correlations are transmitted through a transparent phase sample; the biphoton state undergoes a second-order coherent diffraction effect. This effect can be described as a Fresnel propagator applied to the pump field multiplied by the sample’s transmittance squared. Phase information can thus be observed by collecting defocused coincidence images, provided that a postselection on correlated photon pairs is performed. A quantitative reconstruction of the phase structure can be obtained using phase retrieval methods. We solved numerically the transport of intensity equation using the intensity difference between nearby planes and bench-marked the results by numerical propagation to a third plane where experimental data were available. Phase retrieval techniques are often sensitive to noise, thus long exposure times are usually needed. High-noise images can still be interpreted using image recognition or convolutional neural networks. These approaches will be the subject of our future studies.

#### V. ACKNOWLEDGMENTS

This work was supported by the Canada Research Chair (CRC) Program, NRC-uOttawa Joint Centre for Extreme Quantum Photonics (JCEP) via the Quantum Sensors Challenge Program at the National Research Council of Canada, and Quantum Enhanced Sensing and Imaging (QuEnSI) Alliance Consortia Quantum grant.

- 
- [1] Stephen P Walborn, CH Monken, S Pádua, and PH Souto Ribeiro, “Spatial correlations in parametric down-conversion,” *Physics Reports* **495**, 87–139 (2010).
- [2] Andrew Forbes, Michael De Oliveira, and Mark R Dennis, “Structured light,” *Nature Photonics* **15**, 253–262 (2021).
- [3] Isaac Nape, Bereneice Sephton, Pedro Ornelas, Chane Moodley, and Andrew Forbes, “Quantum structured light in high

- dimensions,” *APL Photonics* **8** (2023).
- [4] Alessio D’Errico and Ebrahim Karimi, “Quantum applications of structured photons,” *Electromagnetic Vortices: Wave Phenomena and Engineering Applications*, 423–455 (2021).
- [5] Marco Barbieri, “Optical quantum metrology,” *PRX Quantum* **3**, 010202 (2022).

- [6] Roy S Bondurant and Jeffrey H Shapiro, “Squeezed states in phase-sensing interferometers,” *Physical Review D* **30**, 2548 (1984).
- [7] Roman Schnabel, “Squeezed states of light and their applications in laser interferometers,” *Physics Reports* **684**, 1–51 (2017).
- [8] Morgan W Mitchell, Jeff S Lundeen, and Aephraem M Steinberg, “Super-resolving phase measurements with a multiphoton entangled state,” *Nature* **429**, 161–164 (2004).
- [9] Guo-Yong Xiang, Brendon Lloyd Higgins, DW Berry, Howard Mark Wiseman, and GJ Pryde, “Entanglement-enhanced measurement of a completely unknown optical phase,” *Nature Photonics* **5**, 43–47 (2011).
- [10] Seongjin Hong, Junaid Ur Rehman, Yong-Su Kim, Young-Wook Cho, Seung-Woo Lee, Hojoong Jung, Sung Moon, Sang-Wook Han, and Hyang-Tag Lim, “Quantum enhanced multiple-phase estimation with multi-mode  $n00n$  states,” *Nature communications* **12**, 5211 (2021).
- [11] L Mandel, *Optical Coherence and Quantum Optics* (Cambridge University Press, 1995).
- [12] Florian Hudelist, Jia Kong, Cunjin Liu, Jietai Jing, ZY Ou, and Weiping Zhang, “Quantum metrology with parametric amplifier-based photon correlation interferometers,” *Nature communications* **5**, 3049 (2014).
- [13] Gaetano Frascella, EE Mikhailov, Naoto Takanashi, RV Zakharov, OV Tikhonova, and MV Chekhova, “Wide-field  $n(1, 1)$  interferometer,” *Optica* **6**, 1233–1236 (2019).
- [14] GS Thekkadath, ME Mycroft, BA Bell, CG Wade, A Eckstein, DS Phillips, RB Patel, A Buraczewski, AE Lita, Thomas Gerrits, *et al.*, “Quantum-enhanced interferometry with large heralded photon-number states,” *NPJ quantum information* **6**, 89 (2020).
- [15] Robin Camphausen, Álvaro Cuevas, Luc Duempelmann, Roland A Terborg, Ewelina Wajs, Simone Tisa, Alessandro Ruggeri, Iris Cusini, Fabian Steinlechner, and Valerio Pruneri, “A quantum-enhanced wide-field phase imager,” *Science Advances* **7**, eabj2155 (2021).
- [16] A Nicholas Black, Long D Nguyen, Boris Braverman, Kevin T Crampton, James E Evans, and Robert W Boyd, “Quantum-enhanced phase imaging without coincidence counting,” *Optica* **10**, 952–958 (2023).
- [17] Miles J Padgett and Robert W Boyd, “An introduction to ghost imaging: quantum and classical,” *Philosophical Transactions of the Royal Society A: Mathematical, Physical and Engineering Sciences* **375**, 20160233 (2017).
- [18] Paul-Antoine Moreau, Ermes Toninelli, Peter A Morris, Reuben S Aspden, Thomas Gregory, Gabriel Spalding, Robert W Boyd, and Miles J Padgett, “Resolution limits of quantum ghost imaging,” *Optics express* **26**, 7528–7536 (2018).
- [19] Yingwen Zhang, Alicia Sit, Frédéric Bouchard, Hugo Larocque, Florence Grenapin, Eliahu Cohen, Avshalom C Elitzur, James L Harden, Robert W Boyd, and Ebrahim Karimi, “Interaction-free ghost-imaging of structured objects,” *Optics express* **27**, 2212–2224 (2019).
- [20] Vincenzo D’ambrosio, Nicolo Spagnolo, Lorenzo Del Re, Sergei Slussarenko, Ying Li, Leong Chuan Kwek, Lorenzo Marrucci, Stephen P Walborn, Leandro Aolita, and Fabio Sciarrino, “Photonic polarization gears for ultra-sensitive angular measurements,” *Nature communications* **4**, 2432 (2013).
- [21] Raouf Barboza, Amin Babazadeh, Lorenzo Marrucci, Filippo Cardano, Corrado de Lisio, and Vincenzo D’Ambrosio, “Ultra-sensitive measurement of transverse displacements with linear photonic gears,” *Nature communications* **13**, 1080 (2022).
- [22] Florence Grenapin, Dilip Paneru, Alessio D’Errico, Vincenzo Grillo, Gerd Leuchs, and Ebrahim Karimi, “Super-resolution enhancement in bi-photon spatial mode demultiplexing,” arXiv preprint arXiv:2212.10468 (2022).
- [23] Hugo Defienne, Bienvenu Ndagano, Ashley Lyons, and Daniele Faccio, “Polarization entanglement-enabled quantum holography,” *Nature Physics* **17**, 591–597 (2021).
- [24] Alice Meda, Elena Losero, Nigam Samantaray, Fabio Scafirimuto, Siva Pradyumna, Alessio Avella, Ivano Ruo-Berchera, and Marco Genovese, “Photon-number correlation for quantum enhanced imaging and sensing,” *Journal of Optics* **19**, 094002 (2017).
- [25] Alois Mair, Alipasha Vaziri, Gregor Weihs, and Anton Zeilinger, “Entanglement of the orbital angular momentum states of photons,” *Nature* **412**, 313–316 (2001).
- [26] David S Simon and Alexander V Sergienko, “Two-photon spiral imaging with correlated orbital angular momentum states,” *Physical Review A—Atomic, Molecular, and Optical Physics* **85**, 043825 (2012).
- [27] Markus Hiekkamäki, Frédéric Bouchard, and Robert Fickler, “Photonic angular superresolution using twisted  $n00n$  states,” *Physical Review Letters* **127**, 263601 (2021).
- [28] Alessio D’Errico, Felix Hufnagel, Filippo Miatto, Mohammadreza Rezaee, and Ebrahim Karimi, “Full-mode characterization of correlated photon pairs generated in spontaneous downconversion,” *Optics Letters* **46**, 2388–2391 (2021).
- [29] Lixiang Chen, Tianlong Ma, Xiaodong Qiu, Dongkai Zhang, Wuhong Zhang, and Robert W Boyd, “Realization of the einstein-podolsky-rosen paradox using radial position and radial momentum variables,” *Physical review letters* **123**, 060403 (2019).
- [30] Kam Wai Clifford Chan, Malcolm N O’Sullivan, and Robert W Boyd, “Two-color ghost imaging,” *Physical Review A—Atomic, Molecular, and Optical Physics* **79**, 033808 (2009).
- [31] Robert Fickler, Mario Krenn, Radek Lapkiewicz, Sven Ramelow, and Anton Zeilinger, “Real-time imaging of quantum entanglement,” *Scientific reports* **3**, 1914 (2013).
- [32] Guillaume Thekkadath, Duncan England, Frédéric Bouchard, Yingwen Zhang, Myungshik Kim, and Benjamin Sussman, “Intensity interferometry for holography with quantum and classical light,” *Science Advances* **9**, eadh1439 (2023), <https://www.science.org/doi/pdf/10.1126/sciadv.adh1439>.
- [33] Danilo Zia, Nazanin Dehghan, Alessio D’Errico, Fabio Sciarrino, and Ebrahim Karimi, “Interferometric imaging of amplitude and phase of spatial biphoton states,” *Nature Photonics* , 1–8 (2023).
- [34] Bienvenu Ndagano, Hugo Defienne, Dominic Branford, Yash D Shah, Ashley Lyons, Niclas Westerberg, Erik M Gauger, and Daniele Faccio, “Quantum microscopy based on hong-ou-mandel interference,” *Nature Photonics* **16**, 384–389 (2022).
- [35] Yingwen Zhang, Duncan England, Andrei Nomerotski, and Benjamin Sussman, “High speed imaging of spectral-temporal correlations in hong-ou-mandel interference,” *Optics Express* **29**, 28217–28227 (2021).
- [36] Xiaoqin Gao, Yingwen Zhang, Alessio D’Errico, Khabat Heshami, and Ebrahim Karimi, “High-speed imaging of spatiotemporal correlations in hong-ou-mandel interference,” *Optics Express* **30**, 19456–19464 (2022).
- [37] Ermes Toninelli, Paul-Antoine Moreau, Thomas Gregory, Adam Mihalysi, Matthew Edgar, Neal Radwell, and Miles Padgett, “Resolution-enhanced quantum imaging by centroid estimation of biphotons,” *Optica* **6**, 347–353 (2019).
- [38] Hugo Defienne, Patrick Cameron, Bienvenu Ndagano, Ashley Lyons, Matthew Reichert, Jiuxuan Zhao, Andrew R Harvey, Edoardo Charbon, Jason W Fleischer, and Daniele Faccio, “Pixel super-resolution with spatially entangled photons,” *Nature communications* **13**, 3566 (2022).

- [39] Yingwen Zhang, Antony Orth, Duncan England, and Benjamin Sussman, “Ray tracing with quantum correlated photons to image a three-dimensional scene,” *Physical Review A* **105**, L011701 (2022).
- [40] Yingwen Zhang, Duncan England, Antony Orth, Ebrahim Karimi, and Benjamin Sussman, “Quantum light-field microscopy for volumetric imaging with extreme depth of field,” *Phys. Rev. Appl.* **21**, 024029 (2024).
- [41] Yingwen Zhang, Duncan England, and Benjamin Sussman, “Snapshot hyperspectral imaging with quantum correlated photons,” *Optics Express* **31**, 2282–2291 (2023).
- [42] Xiaoqin Gao, Yingwen Zhang, Alessio D’Errico, Alicia Sit, Khabat Heshami, and Ebrahim Karimi, “Full spatial characterization of entangled structured photons,” *Physical Review Letters* **132**, 063802 (2024).
- [43] Nazanin Dehghan, Alessio D’Errico, Francesco Di Colandrea, and Ebrahim Karimi, “Biphoton state reconstruction via phase retrieval methods,” *Optica* **11**, 1115–1123 (2024).
- [44] Eliot Bolduc, Daniele Faccio, and Jonathan Leach, “Acquisition of multiple photon pairs with an emccd camera,” *Journal of Optics* **19**, 054006 (2017).
- [45] Bruno Eckmann, Bänz Bessire, Manuel Unternährer, Leonardo Gasparini, Matteo Perenzoni, and André Stefanov, “Characterization of space-momentum entangled photons with a time resolving cmos spad array,” *Optics express* **28**, 31553–31571 (2020).
- [46] Andrei Nomerotski, Matthew Chekhlov, Denis Dolzhenko, Rene Glazenberg, Brianna Farella, Michael Keach, Ryan Mahon, Dmitry Orlov, and Peter Svihra, “Intensified tpx3cam, a fast data-driven optical camera with nanosecond timing resolution for single photon detection in quantum applications,” *Journal of Instrumentation* **18**, C01023 (2023).
- [47] Sanjukta Kundu, Jerzy Szuniewicz, Grzegorz Firlik, Alexander Krupinski-Ptaszek, and Radek Lapkiewicz, “High-dimensional quantum correlation measurements with an adaptively gated hybrid single-photon camera,” *Optica Quantum* **2**, 206–213 (2024).
- [48] Chloé Vernière and Hugo Defienne, “Hiding images in quantum correlations,” *Physical Review Letters* **133**, 093601 (2024).
- [49] Hugo Larocque, Jérémie Gagnon-Bischoff, Frédéric Bouchard, Robert Fickler, Jeremy Upham, Robert W Boyd, and Ebrahim Karimi, “Arbitrary optical wavefront shaping via spin-to-orbit coupling,” *Journal of Optics* **18**, 124002 (2016).
- [50] T. M. Godden, A. Muniz-Piniella, J. D. Claverley, A. Yacoot, and M. J. Humphry, “Phase calibration target for quantitative phase imaging with ptychography,” *Opt. Express* **24**, 7679–7692 (2016).
- [51] Chao Zuo, Jiaji Li, Jiasong Sun, Yao Fan, Jialin Zhang, Linpeng Lu, Runnan Zhang, Bowen Wang, Lei Huang, and Qian Chen, “Transport of intensity equation: a tutorial,” *Optics and Lasers in Engineering* **135**, 106187 (2020).
- [52] Giuseppe Ortolano, Alberto Paniate, Pauline Boucher, Carmine Napoli, Sarika Soman, Silvania F Pereira, Ivano Ruo-Berchera, and Marco Genovese, “Quantum enhanced non-interferometric quantitative phase imaging,” *Light: Science & Applications* **12**, 171 (2023).

**Author Contributions** N.D. and A.D. conceived the idea. N.D., A.D and Y.Z. performed the experiment. Y.Z. prepared the code for the data analysis and A.D. for the centroid coincidence extraction. N.D. and A.D. analyzed the data. E.K. supervised the project. A.D. prepared the first version of the manuscript. All authors contributed to the writing of the manuscript.

**Data availability** The data that support the findings of this study are available from the corresponding author upon reasonable request.

**Code availability** The code used for the data analysis is available from the corresponding author upon reasonable request.

**Ethics declarations** Competing Interests. The authors declare no competing interests.

**Corresponding authors** Correspondence and requests for materials should be addressed to aderrico@uottawa.ca.